NASA TN D-1056

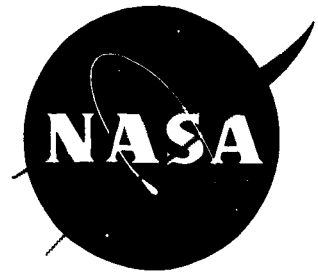

TECHNICAL NOTE

D-1056

PRELIMINARY BASE PRESSURES OBTAINED FROM THE X-15 AIRPLANE AT MACH NUMBERS FROM 1.1 TO 3.2

By Edwin J. Saltzman

Flight Research Center
Edwards, Calif.

NATIONAL AERONAUTICS AND SPACE ADMINISTRATION

WASHINGTON

August 1961

NATIONAL AERONAUTICS AND SPACE ADMINISTRATION

TECHNICAL NOTE D-1056

PRELIMINARY BASE PRESSURES OBTAINED FROM THE X-15 AIRPLANE AT MACH NUMBERS FROM 1.1 TO 3.2

By Edwin J. Saltzman

SUMMARY

Base pressure measurements have been made on the fuselage, 10°-wedge vertical fin, and side fairing of the X-15 airplane. Data are presented for Mach numbers between 1.1 and 3.2 for both powered and unpowered flight. Comparisons are made with data from small-scale-model tests, semiempirical estimates, and theory.

The results of this preliminary study show that operation of the interim rocket engines (propellant flow rate approximately 70 lb/sec) reduces the base drag of the X-15 by 25 to 35 percent throughout the test Mach number range.

Values of base drag coefficient for the side fairing and fuselage obtained from X-15 wind-tunnel models were adequate for predicting the overall full-scale performance of the test airplane.

The leading-edge sweep of the upper movable vertical fin was not an important factor affecting the fin base pressure.

The power-off base pressure coefficients of the upper movable vertical fin (a 10° wedge with chord-to-thickness ratio of 5.5 and semispan-to-thickness ratio of 3.2) are in general agreement with the small-scale blunt-trailing-edge-wing data of several investigators and with two-dimensional theory.

INTRODUCTION

Information on full-scale base pressure characteristics is of interest to the aircraft designer. Many future aircraft, especially boost gliders, will operate over extremely large speed ranges, from many times the speed of sound to landing speeds. Smooth aerodynamic lines

will sometimes have to be compromised in favor of stability, control, or propulsion requirements. For some vehicles this will result in blunt trailing edges on stabilizing surfaces, or, as for a boost glider, a blunt fuselage base may remain after separation from the final booster. Such abrupt changes in cross-sectional area add significantly to the base drag of a vehicle.

Small-scale base pressure experiments have been performed by many investigators. The results of several such studies are summarized and supplemented in reference 1. The X-15 airplane now provides an opportunity to complement these small-scale tests with full-scale base pressure data. The X-15 is of interest from the standpoint of base pressures, inasmuch as: (1) the base area is unusually large, about 80 percent of the total frontal area; (2) data from the 10°-wedge vertical fin are available, as well as fuselage data; and (3) both power-on and power-off results can be obtained.

This paper is concerned with the base pressure measured on the fuselage, side fairing, and the 10°-wedge vertical fin of the X-15 during tests conducted at the NASA Flight Research Center, Edwards, Calif.

SYMBOLS

A base-element area, sq ft

$b/2$ semispan, ft

C_{D_b} base drag coefficient for each base element, $-C_p \frac{A}{S}$

$C_{D_{b_t}}$ total of base drag coefficients of vertical fins, side fairings, and fuselage

$$\Delta C_{D_{b_t}} = \left(C_{D_{b_t}}\right)_{off} - \left(C_{D_{b_t}}\right)_{on}$$

C_{D_0} overall zero-lift drag coefficient, $\frac{D}{qS}$

C_p base pressure coefficient, $\frac{p_b - p}{q}$

C_{p_v} absolute limit of base pressure coefficient, zero base pressure, $\frac{-p}{q}$

c	chord of wing, fin, or other appropriate length, ft
D	drag force along flight path, lb
d	axial distance forward from mean exhaust exit station to pressure orifice, in.
h	trailing-edge thickness of wing or fin, ft
h_p	pressure altitude, ft
M	free-stream Mach number
p	free-stream static pressure, lb/sq ft
p_b	base static pressure, lb/sq ft
q	free-stream dynamic pressure, $0.7M^2p$, lb/sq ft
R	free-stream Reynolds number, $\frac{\rho Vc}{\mu}$
R_{ft}	free-stream Reynolds number per foot, $\frac{\rho V}{\mu}$
S	wing area, sq ft
t	maximum wing or fin thickness, ft
V	true airspeed, ft/sec
α	angle of attack, deg
β	angle of sideslip, deg
δ_h	horizontal control-surface deflection, deg
δ_j	speed-brake deflection, deg
δ_v	vertical control-surface deflection, deg
μ	absolute viscosity, lb-sec/sq ft
ρ	air density, slugs/cu ft
Λ	leading-edge sweep angle, deg

Subscripts:

off	rocket engines not thrusting (power off)

on rocket engines thrusting (power on)

1 . . . 9 orifice numbers (table II)

AIRPLANE

General Description

The North American X-15 is a single-place, low-aspect-ratio monoplane (figs. 1 and 2) designed for manned flight research at maximum speeds on the order of 6,600 feet per second. When design speed is achieved, the X-15 will be propelled by a single XLR99 rocket engine providing approximately 58,000 pounds of thrust. For the data presented in this paper the airplane was powered by interim engines, consisting of a cluster of eight LR11 rocket chambers, which provided a combined thrust of about 16,000 pounds at flight conditions. Although only about one-half of the design speed can be obtained with the interim engines, the performance thus far is in excess of that achieved by any other airplane.

The X-15 is carried to an altitude of about 45,000 feet by a B-52 carrier airplane and is then launched at a Mach number of approximately 0.8. The interim engines provide slightly more than 4 minutes of powered flight, after which the airplane glides to a landing on the dry lakebed at Edwards Air Force Base, Calif.

Base and Exhaust-Jet Details

A view of the airplane from the rear is shown in figure 3, and a view of the aft portion of the fuselage from left of center is shown in figure 4. Both of these figures show that the base regions formed by the closed speed brakes are open to the rear instead of having base surfaces. In addition, it may be seen in figure 4 that, relative to the fuselage centerline, the four upper chambers are canted up and the four lower chambers are canted down. This relative inclination amounts to between 2.0° and 2.5° in the X-Z plane. Also shown in figure 4 is the relative axial displacement of the fuselage, vertical fin, and side-fairing bases. For the present tests the jettisonable portion of the lower vertical fin was attached; however, it is always jettisoned before landing to provide necessary ground clearance (see fig. 4).

General physical characteristics of the airplane are presented in table I. Dimensions pertinent to the present tests are given in the following tabulation:

	Power off	Power on
Base-element area, sq ft:		
Upper movable vertical fin	4.7	4.7
Lower movable vertical fin (jettisonable portion)	3.4	3.4
Stationary portion of vertical fins (both)	6.7	6.7
Side fairings (both)	4.8	4.8
Fuselage	11.5	9.5
Total base area, sq ft	31.1	29.1
Fuselage boattail angle, deg		6
Upper movable vertical fin, ft:		
Mean chord		8.46
Mean trailing-edge thickness		1.55
Axial distance, d, in.:		
Orifices 1, 2, 3, 4, and 9		35
Orifice 5		10
Orifice 6		3.5
Orifice 7		10
Orifice 8		44
Engine:		
Number of chambers		8
Throat area of nozzles (each), sq in.		4.8
Exit area of nozzles (each), sq in.		35.5
Exit area of turbine exhaust (one of two), sq in.		3.9
Chamber pressure (nominal), psia		260
Exit pressure (nominal), psia		4 to 6

INSTRUMENTATION

The location of each orifice used to measure base pressure is shown in figure 5. Although nine locations are shown, only seven orifices could be used for each of the two flights on which base pressure data were obtained (see table II). The orifices were connected to aneroid-type differential cells mounted in a standard NASA 24-cell photographic recording manometer.

Free-stream total pressure and free-stream static pressure were sensed from nose-boom stations located slightly more than 1 fuselage diameter ahead of the airplane nose. Other parameters pertinent to this paper were measured on standard NASA flight data-recording instruments, and all records were synchronized by a common timer.

ACCURACY

The maximum error in base pressure coefficient is considered to be within ±0.02. The maximum error in Mach number is about ±0.02 for Mach numbers between 1 and 2 and about ±0.03 for Mach numbers between 2 and 3.

TEST CONDITIONS

Base pressure data were obtained from two flights over a Mach number range of 1.1 to 3.2 and an altitude range from about 39,000 feet to 80,000 feet. Free-stream Reynolds number varied between 0.8 million and 2.6 million per foot. The following table lists the test Reynolds numbers for the various base elements, as well as Reynolds number values for the small-scale model data used later for comparison purposes.

Investigation	$R_{ft} \times 10^{-6}$	$R \times 10^{-6}$	Based on -	Representative length, ft
Present tests (power on and power off)	0.8 to 2.6	6.8 to 22.0	Upper movable vertical fin	8.46
		38.3 to 124.5	Side fairing	47.90
		40.6 to 132.0	Fuselage	50.75
Reference 2	3.8	11.9	Side fairing	3.13
Reference 3	2.7	8.9	Fuselage	3.28
Reference 4	4.0 to 4.7	3.9 to 4.6	Fuselage	.98
Reference 5	6.2 to 9.6	1.3 to 1.8	Wing chord	.19 to .21
Reference 6	6.8 to 14.0	1.7 to 3.5	Wing chord	.25
Reference 7	----------	1 to 10	Wing chord	----------

The X-15 has many protuberances scattered over the fuselage, and in some areas of the fuselage and vertical fins the surfaces are wavy. Unpublished heat-transfer data indicate that with the exception of localized laminar areas on the wings and lower vertical fin, the flow over the X-15 was primarily turbulent for the present tests. Preliminary measurements made at midsemispan for the upper vertical fin indicate less than 1 foot of laminar flow near a Mach number of 3.

The jettisonable portion of the lower vertical fin was attached throughout the present tests. Other conditions which existed during these tests are presented in table II.

DISCUSSION OF RESULTS

Full-Scale Data

The basic data obtained in this investigation and supplementary information are listed in table II. For the fuselage or the vertical fin, where more than one pressure was recorded, an arithmetic mean value of the base pressure coefficient C_p is used in the figures to represent the respective base element.

In this investigation it was determined that angle of attack was not a large factor in the definition of base pressure coefficient (also shown in ref. 1). In addition, the effects of Reynolds number over the test range should be small because turbulent boundary-layer conditions existed upstream of the bases, as noted in the TEST CONDITIONS section. For these reasons the basic data in figures 6 and 7 are plotted together irrespective of angle of attack or Reynolds number.

Figures 6 and 7 show the relationship of base pressure coefficient to Mach number for power-off and power-on conditions, respectively. In figure 6 it can be seen that extended speed brakes cause the base pressure coefficients to increase negatively for the vertical fin and side fairing. Deflection of the speed brakes has little effect on flow characteristics over the fuselage base, as indicated by the small change in fuselage base pressure coefficients accompanying speed-brake deflection.

The data of figures 6 and 7 are faired and compared in figure 8 to show the effect of engine operation. It is apparent throughout most of the Mach number range that engine operation significantly affects the fuselage and vertical-fin coefficients, but, has a much smaller effect on the side fairing. The following table gives a brief summary of these power-on effects:

Base elements	$\frac{C_{p_{on}}}{C_{p_{off}}}$		
	M = 1.2	M = 2.2	M = 3.2
Vertical fin	0.77	0.82	0.88
Side fairing	.94	1.07	.92
Fuselage	.75	.46	.47

The changes in the slope of the curve of base pressure coefficient and Mach number in figures 6 to 8 are believed to be dependent on local effects. A more comprehensive study with greater control over the variables would be necessary to verify and explain these slope changes.

The effect of base pressure on the drag of each of the three base-area elements is shown in figure 9 for power-off and power-on conditions. Comparison of the two conditions shows that the side fairing contributes about the same amount of drag regardless of engine operation, whereas both the vertical-fin and the fuselage bases experience a significant reduction in drag when the engines are operating.

The total base drag of all of the base elements is presented in figure 10 for both power-off and power-on conditions. Also shown is the incremental difference between power-off and power-on total base drag $\Delta C_{D_{bt}}$, which is 25 to 35 percent of the total power-off base drag.

The ratio of power-off total base drag $C_{D_{bt}}$ to power-off overall airplane drag for zero lift C_{D_0} is shown in figure 11. Base drag is about 45 percent of C_{D_0} for a Mach number of 1.2 and decreases to about 30 percent at $M = 3.0$.

Comparison With Results of Other Investigations

Wind-tunnel models of X-15.- Figure 12 is a comparison of base drag coefficients obtained from full-scale flight and X-15 model data. Model data are available for the fuselage and side-fairing bases, but not for the vertical-fin base. Comparisons with the side-fairing data of reference 2 and the fuselage-base results of references 3 and 4 indicate agreement adequate for predicting the overall full-scale performance of the X-15 airplane, even though the discrepancy reaches 10 to 15 percent of the drag coefficient for the respective bases over much of the Mach number range. The model bases were not dimensionally exact; however, the model drag coefficients as presented herein are adjusted to base areas corresponding to exact models.

Blunt-trailing-edge-wing results.- Base pressure characteristics of the upper movable vertical fin (fig. 3) are compared with two-dimensional results of other investigations in the following discussion.

Reference 5 discusses possible effects of leading- and trailing-edge sweep on the base pressure of blunt-trailing-edge wings. Because the X-15 upper vertical fin has 30° of leading-edge sweep, the effects of sweep were investigated. In reference 5 it was found that base pressure data from untapered wings with and without leading-edge sweep correlated well when plotted as a function of $M \cos \Lambda$. An exception was data at $M \approx 2$ for a tapered delta wing with 45° sweep, which suggested that the M component normal to the trailing edge may be more important as a correlating parameter than $M \cos \Lambda$. This is shown by the flagged and unflagged solid symbols in figure 13. A similar result is shown in figure 13 for the upper movable vertical fin (circular and square symbols). The circular symbols are plotted with $M \cos \Lambda$ as the

abscissa, where Λ for the unflagged circles includes the structural sweep of the fin and angle of attack and Λ for the flagged circles includes only the structural sweep. (The true $M \cos \Lambda$ should fall somewhere between the limits established by the unflagged and flagged circular symbols.) The square symbols are plotted with M as the abscissa, disregarding both leading-edge structural sweep and angle of attack. As can be seen, the squares provide better correlation with the unswept experimental results of references 5 and 6, the delta-wing data plotted against M, and the two-dimensional theory of reference 8.[a] This indicates that either free-stream Mach number or the M component normal to the trailing edge is a more important correlating parameter than the Mach number component normal to the leading edge. From the present results it cannot be determined which parameter, free-stream Mach number or the M component normal to the trailing edge, is the one most important correlating factor.

The departure of the fin data from the levels of references 6 and 8 (fig. 13) at the higher Mach numbers (also evident in fig. 14) may be related to a shock environment originating upstream of the entire fin. Local-flow effects such as those mentioned in conjunction with figures 6 to 8 may also be influencing factors.

Because figure 13 showed that the leading-edge sweep of the upper movable vertical fin was not an important factor affecting base pressure, the comparisons which follow are made with configurations having no sweep.

Figure 14 compares full-scale base pressure-coefficient data for the upper movable vertical fin with two-dimensional results of several investigations. The comparison data include semiempirical estimates from figure 5 of reference 1,[b] experimental blunt-trailing-edge-wing data compiled from several sources by Hoerner (ref. 7), and the two-dimensional theory of reference 8. As can be seen, the full-scale fin data are in general agreement with all of the two-dimensional comparison data, although some divergence is apparent at Mach numbers above 2.5. In contrast, the base pressure coefficient for a body of revolution without boattail or fins would be about 60 percent of the two-dimensional values for $M \approx 2$.

Another example of the two-dimensional nature of flow over the upper movable vertical fin is obtained by using reference 6. It was

[a]This theory is based on the concepts of interaction between the dissipative shear flow and the adjacent free stream and the conservation of mass in the wake. Pressure coefficient is referenced to conditions immediately ahead of the base.

[b]Estimates are based on an analogy to the peak pressure rise associated with the separation of a turbulent boundary layer on a flat plate caused by a forward-facing step. Pressure coefficient is referenced to conditions immediately ahead of the base.

established in reference 6 that, for a given Mach number, the curve $\frac{p_b}{p}$ plotted against $\frac{c}{h(R)^{1/5}}$ was sufficient for correlating numerous blunt-trailing-edge wings varying in thickness from 5 to 10 percent and ranging from positive to negative boattail angles. These small-scale results representing ratios of semispan to trailing-edge thickness $\frac{b/2}{h}$ from 15 to 120 are compared in figure 15 with results from the upper movable vertical fin which has a corresponding ratio of 3.2. The ratios of the chord-to-trailing-edge thickness $\frac{c}{h}$ for the model data varied from 10 to 80, as compared to a mean value of 5.5 for the upper movable vertical fin. With the probable increasing use of blunt-trailing-edge wings and control surfaces in the design of future aircraft, it is of interest that configurations so different in $\frac{b/2}{h}$, $\frac{c}{h}$, and scale possess similar base pressure characteristics.

CONCLUDING REMARKS

A preliminary study of base pressure characteristics for the X-15 airplane indicates that:

1. Operation of the interim rocket engines (propellant flow rate approximately 70 lb/sec) reduces the base drag of the X-15 by 25 to 35 percent throughout the test Mach number range.

2. Values of base drag coefficient for the side fairing and fuselage obtained from X-15 wind-tunnel models were adequate for predicting the overall full-scale performance of the test airplane.

3. The leading-edge sweep of the upper movable vertical fin was not an important factor affecting the fin base pressure.

4. The power-off base pressure coefficients of the upper movable vertical fin (a 10° wedge with chord-to-thickness ratio of 5.5 and semispan-to-thickness ratio of 3.2) are in general agreement with small-scale blunt-trailing-edge-wing data of several investigators and with two-dimensional theory.

Flight Research Center,
National Aeronautics and Space Administration,
Edwards, Calif., March 24, 1961

REFERENCES

1. Love, Eugene S.: Base Pressure at Supersonic Speeds on Two-Dimensional Airfoils and on Bodies of Revolution With and Without Fins Having Turbulent Boundary Layers. NASA TN 3819, 1957. (Supersedes RM L53C02.)

2. Franklin, Arthur E., and Silvers, H. Norman: Investigation of the Aerodynamic Characteristics of a 0.067-Scale Model of the X-15 Airplane (Configuration 2) at Mach Numbers of 2.29, 2.98, 3.96, and 4.65. NASA MEMO 4-27-59L, 1959.

3. Franklin, Arthur E., and Lust, Robert M.: Investigation of the Aerodynamic Characteristics of a 0.067-Scale Model of the X-15 Airplane (Configuration 3) at Mach Numbers of 2.29, 2.98, and 4.65. NASA TM X-38, 1959.

4. Leupold, Mathias J., and Freeman, Elizabeth M.: A Second Series of Supersonic Force Tests on the Full-Span Model X-15 for North American Aviation Incorporated. WTR 200, Mass. Inst. of Tech. (Naval Supersonic Laboratory), Sept. 1958.

5. Goin, Kennith L.: Effects of Plan Form Airfoil Section, and Angle of Attack on the Pressures Along the Base of Blunt-Trailing-Edge Wings at Mach Numbers of 1.41, 1.62, and 1.96. NACA RM L52D21, 1952.

6. Chapman, Dean R., Wimbrow, William R., and Kester, Robert H.: Experimental Investigation of Base Pressure on Blunt-Trailing-Edge Wings at Supersonic Velocities. NACA Rep. 1109, 1952. (Supersedes TN 2611.)

7. Hoerner, Sighard F.: Fluid-Dynamic Drag. Pub. by the author (148 Busteed, Midland Park, N. J.), 1958, ch. XVI, p. 11.

8. Korst, H. H.: A Theory for Base Pressures in Transonic and Supersonic Flow. Jour. App. Mech., vol. 23, no. 4, Dec. 1956, pp. 593-598.

TABLE I.- PHYSICAL CHARACTERISTICS OF THE AIRPLANE

Wing:	
Airfoil section	NACA 66005 (Modified)
Total area (includes 94.98 sq ft covered by fuselage), sq ft	200
Span, ft	22.36
Mean aerodynamic chord, ft	10.27
Root chord, ft	14.91
Tip chord, ft	2.98
Taper ratio	0.20
Aspect ratio	2.50
Sweep at 25-percent-chord line, deg	25.64
Incidence, deg	0
Dihedral, deg	0
Aerodynamic twist, deg	0
Flap -	
Type	Plain
Area (each), sq ft	8.30
Span (each), ft	4.50
Inboard chord, ft	2.61
Outboard chord, ft	1.08
Deflection, down, deg	40
Ratio flap chord to wing chord	0.22
Ratio total flap area to wing area	0.08
Ratio flap span to wing semispan	0.40
Trailing-edge angle, deg	5.67
Sweepback angle of hinge line, deg	0
Horizontal tail:	
Airfoil section	NACA 66005 (Modified)
Total area (includes 63.29 sq ft covered by fuselage), sq ft	115.34
Span, ft	18.08
Mean aerodynamic chord, ft	7.05
Root chord, ft	10.22
Tip chord, ft	2.11
Taper ratio	0.21
Aspect ratio	2.83
Sweep at 25-percent-chord line, deg	45
Dihedral, deg	-15
Ratio horizontal-tail area to wing area	0.58
Movable surface area, sq ft	51.77
Deflection -	
Longitudinal, up, deg	15
Longitudinal, down, deg	35
Lateral differential (pilot authority), deg	±15
Lateral differential (autopilot authority), deg	±30
Control system	Irreversible hydraulic boost with artificial feel

TABLE I.- PHYSICAL CHARACTERISTICS OF THE AIRPLANE - Concluded

Upper vertical tail:	
Airfoil section	10° single wedge
Total area, sq ft	40.91
Span, ft	4.58
Mean aerodynamic chord, ft	8.95
Root chord, ft	10.21
Tip chord, ft	7.56
Taper ratio	0.74
Aspect ratio	0.51
Sweep at 25-percent-chord line, deg	23.41
Ratio vertical-tail area to wing area	0.20
Movable surface area, sq ft	26.45
Deflection, deg	±7.50
Sweepback of hinge line, deg	0
Control system	Irreversible hydraulic boost with artificial feel
Lower vertical tail:	
Airfoil section	10° single wedge
Total area, sq ft	34.41
Span, ft	3.83
Mean aerodynamic chord, ft	9.17
Root chord, ft	10.21
Tip chord, ft	8
Taper ratio	0.78
Aspect ratio	0.43
Sweep at 25-percent-chord line, deg	23.41
Ratio vertical-tail area to wing area	0.17
Movable surface area, sq ft	19.95
Deflection, deg	±7.50
Sweepback of hinge line, deg	0
Control system	Irreversible hydraulic boost with artificial feel
Fuselage:	
Length, ft	50.75
Maximum width, ft	7.33
Maximum depth, ft	4.67
Maximum depth over canopy, ft	4.97
Side area (total), sq ft	215.66
Fineness ratio	10.91
Speed brake:	
Area (each), sq ft	5.37
Mean span (each), ft	1.60
Chord (each), ft	3.36
Deflection, deg	35
Frontal area at maximum deflection, sq ft	13.8
Base area (fuselage, side fairings, vertical fins), sq ft	31.1
Total frontal area (maximum) including wing and horizontal tail at 0° deflection, sq ft	38.8

TABLE II.- SUPPLEMENTARY INFORMATION

Flight	Time	No. of chambers burning	M	$\frac{h_p}{1000}$, ft	q, psf	$R_{ft} \times 10^{-6}$	δ_v, deg	δ_h, deg	δ_j, deg	α, deg	β, deg	C_{p_1}	C_{p_2}	C_{p_3}	C_{p_4}	C_{p_5}	C_{p_6}	C_{p_7}	C_{p_8}	C_{p_9}
	130.0	8	1.17	38.9	396	2.34	-1.1	-6.8	Closed	9.5	-0.7	-----	-0.306	-----	-0.250	-0.237	-0.218	-0.283	-0.362	-0.205
	145.0	8	1.22	39.2	425	2.42	----	-6.4	↓	8.3	----	-----	-.322	-----	-.261	-.239	-.198	-.260	-.339	-.204
	215.0	8	1.35	57.1	222	1.15	-.9	-7.9		6.8	-.5	-----	-.262	-----	-.227	-.170	-.121	-.211	-.307	-.218
	235.0	8	1.52	58.8	260	1.17	-.8	-11.9		8.3	-.5	-----	-.206	-----	-.203	-.128	-.112	-.177	-.266	-.206
	265.0	8	1.81	61.5	322	1.24	-.8	-14.0		8.5	-.4	-----	-.167	-----	-.181	-.108	-.096	-.132	-.221	-.178
	305.0	8	2.14	71.9	274	.88	-1.0	-13.6		7.9	-.8	-----	-.147	-----	-.147	-.064	-.071	-.086	-.176	-.121
	325.0	8	2.46	77.7	274	.81	-1.3	-1.9		7.4	-1.1	-----	-.128	-----	-.126	-.042	-.056	-.068	-.116	-.112
	342.0	8	2.87	76.0	407	.98	-1.0	-6.0		2.5	-.7	-----	-.115	-----	-.109	-.044	-.052	-.056	-.095	-.093
	356.0	8	3.24	69.7	700	1.49	-1.2	-6.2		3.6	-1.0	-----	-.114	-----	-.095	-.048	-.052	-.055	-.082	-.087
	366.0	0	3.24	64.3	904	1.93	-.6	-7.3		4.1	-.9	-----	-.120	-----	-.109	-.097	-.097	-.107	-.088	-.102
A	369.0	0	3.16	62.8	925	2.02	-.6	-14.1		7.2	-.7	-----	-.127	-----	-.116	-.103	-.103	-.114	-.100	-.098
	371.0	0	3.11	62.3	914	2.05	-.6	-18.3		10.5	-.5	-----	-.134	-----	-.121	-.107	-.107	-.114	-.105	-.091
	380.5	0	2.80	60.7	845	1.99	-.6	-5.4		3.5	-.5	-----	-.150	-----	-.134	-.123	-.123	-.128	-.102	-.128
	401.5	0	2.45	58.1	697	1.96	-.2	-18.6		10.0	-.5	-----	-.173	-----	-.160	-.154	-.156	-.172	-.160	-.146
	409.5	0	2.15	58.3	528	1.63	.5	-12.8		7.1	-.3	-----	-.201	-----	-.194	-.182	-.180	-.193	-.174	-.198
	435.5	0	1.80	55.2	431	1.66	-.4	-4.7		4.8	-.4	-----	-.247	-----	-.246	-.201	-.202	-.220	-.191	-.256
	435.9	0	1.80	55.1	431	1.66	-.4	-4.7		3.1	-.4	-----	-.251	-----	-.247	-.203	-.206	-.229	-.191	-.258
	436.2	0	1.79	55.0	431	1.66	-.4	-4.9		1.2	-.3	-----	-.249	-----	-.247	-.199	-.204	-.226	-.190	-.258
	456.5	0	1.68	46.7	563	2.36	-.1	-5.2		2.0	-.1	-----	-.289	-----	-.272	-.211	-.208	-.236	-.208	-.265
	465.0	0	1.52	43.1	552	2.51	-.2	-5.2		3.3	-.2	-----	-.307	-----	-.299	-.218	-.226	-.246	-.246	-.301
	474.0	0	1.35	39.8	504	2.63	-.4	-6.2		5.4	-.3	-----	-.324	-----	-.316	-.254	-.262	-.281	-.308	-.312
	479.6	0	1.23	37.9	461	2.58	-.4	-6.8		7.8	-.3	-----	-.406	-----	-.324	-.274	-.284	-.319	-.362	-.328
	483.0	0	1.15	36.9	418	2.53	-.4	-6.5		8.5	-.3	-----	-.443	-----	-.347	-.316	-.314	-.374	-.404	-.325
	148.0	8	1.08	42.0	289	1.89	0.3	-6.3	Closed	10.1	-0.4	-0.276	-0.299	-0.324	-0.272	-0.237	-0.218	-----	-0.420	-----
	238.0	8	1.31	54.1	240	1.28	-.3	-6.5	↓	8.6	.2	-.263	-.299	-.297	-.277	-.179	-.161	-----	-.338	-----
	278.0	8	1.51	63.1	207	.95	.2	-11.2		7.5	-.3	-.250	-.227	-.274	-.238	-.116	-.127	-----	-.288	-----
	303.0	8	1.81	63.8	290	1.11	.1	-13.9		8.4	-.1	-.219	-.200	-.233	-.212	-.115	-.131	-----	-.237	-----
	348.0	8	2.27	71.7	311	.99	.3	-15.3		8.6	-.9	-.176	-.175	-.171	-.167	-.073	-.091	-----	-.188	-----
	366.5	8	2.51	77.7	287	.82	.2	-6.1		5.5	-.7	-.140	-.138	-.142	-.152	-.039	-.068	-----	-.137	-----
	367.7	8	2.54	78.1	287	.80	.2	-5.6		.9	0	-.146	-.140	-.141	-.154	-.039	-.074	-----	-.137	-----
	368.9	8	2.55	78.2	289	.79	.2	-5.6		4.9	-.5	-.140	-.137	-.145	-.145	-.042	-.067	-----	-.140	-----
	375.5	8	2.70	79.4	306	.78	.2	-5.4		2.2	-.3	-.136	-.125	-.134	-.134	-.037	-.069	-----	-.122	-----
	387.2	8	2.99	79.5	374	.86	.1	-8.0		2.4	-.2	-.120	-.117	-.123	-.109	-.039	-.048	-----	-.109	-----
B	395.0	8	3.19	78.0	455	1.00	.1	-5.9		3.8	-.5	-.121	-.105	-.112	-.103	-.030	-.052	-----	-.094	-----
	404.0	0	3.17	75.7	501	1.10	.3	-14.8		8.7	.6	-.136	-.129	-.136	-.125	-.084	-.095	-----	-.109	-----
	418.5	0	2.95	73.9	474	1.10	.4	-4.1		2.2	0	-.156	-.149	-.138	-.138	-.107	-.127	-----	-.100	-----
	441.0	0	2.66	69.3	478	1.25	.3	-5.9		3.0	0	-.183	-.169	-.170	-.164	-.129	-.146	-----	-.120	-----
	448.0	0	2.56	68.5	461	1.25	.4	-2.1		1.1	-.2	-.190	-.179	-.166	-.167	-.142	-.154	-----	-.120	-----
	467.2	0	2.30	62.2	502	1.52	.4	-13.1		8.3	.1	-.191	-.189	-.187	-.190	-.167	-.187	-----	-.166	-----
	483.0	0	1.97	59.4	422	1.49	.3	-7.8		4.4	0	-.248	-.228	-.253	-.246	-.200	-.206	-----	-.197	-----
	493.4	0	1.81	57.0	398	1.54	.3	-8.4	35°	4.5	-.3	-.346	-.328	-.302	-.324	-.205	-.226	-----	-.263	-----
	496.0	0	1.70	55.5	381	1.55	.2	-8.6	35°	4.6	-.2	-.390	-.370	-.339	-.366	-.233	-.249	-----	-.312	-----
	508.0	0	1.52	52.5	352	1.60	.2	-8.4	Closed	5.2	-.2	-.347	-.322	-.353	-.308	-.210	-.238	-----	-.261	-----
	522.4	0	1.31	47.8	324	1.74	.2	-9.9	↓	8.5	-.3	-.333	-.378	-.396	-.332	-.246	-.276	-----	-.346	-----
	533.0	0	1.09	46.1	246	1.58	.1	-7.4		10.2	-.5	-.353	-.437	-.429	-.359	-.310	-.329	-----	-.448	-----

Figure 1.- Photograph of the X-15 airplane. E-5250

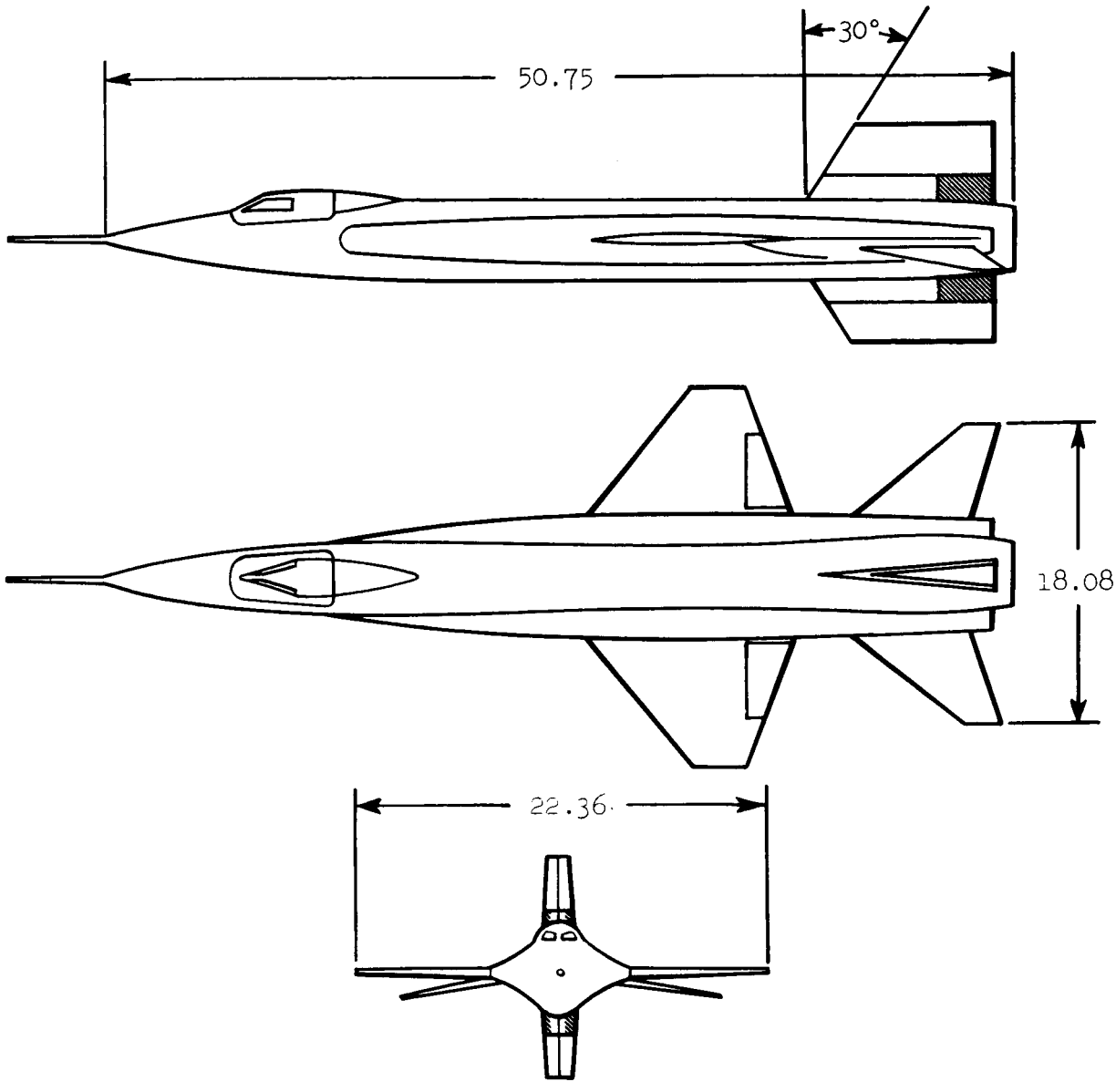

Figure 2.- Three-view drawing of the X-15 airplane. All dimensions in feet, except as noted. Speed brakes shown crosshatched.

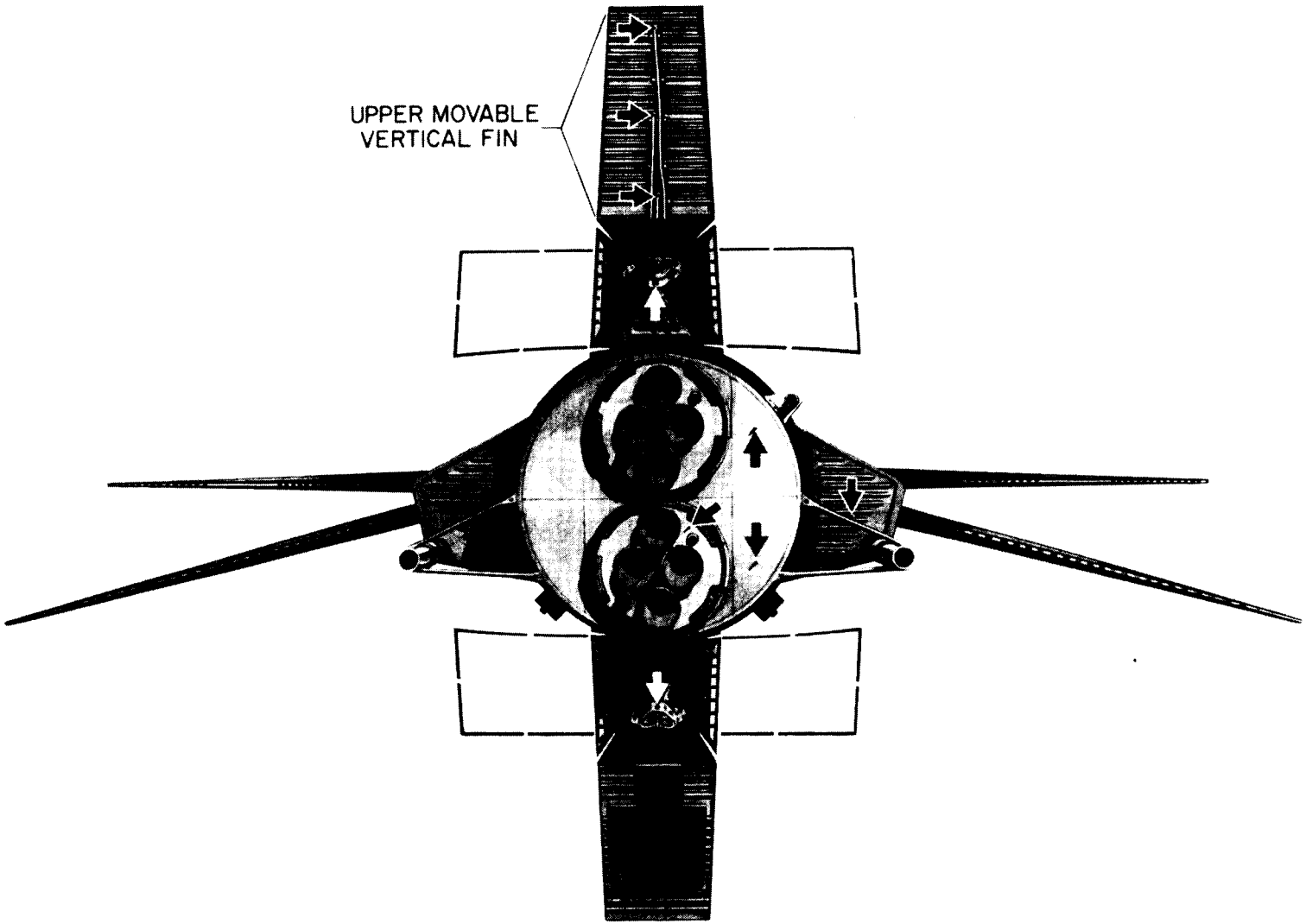

Figure 3.- Rear view of X-15 airplane. Locations of pressure orifices are indicated by arrows. Position of speed brakes when open shown by broken lines. E-6645

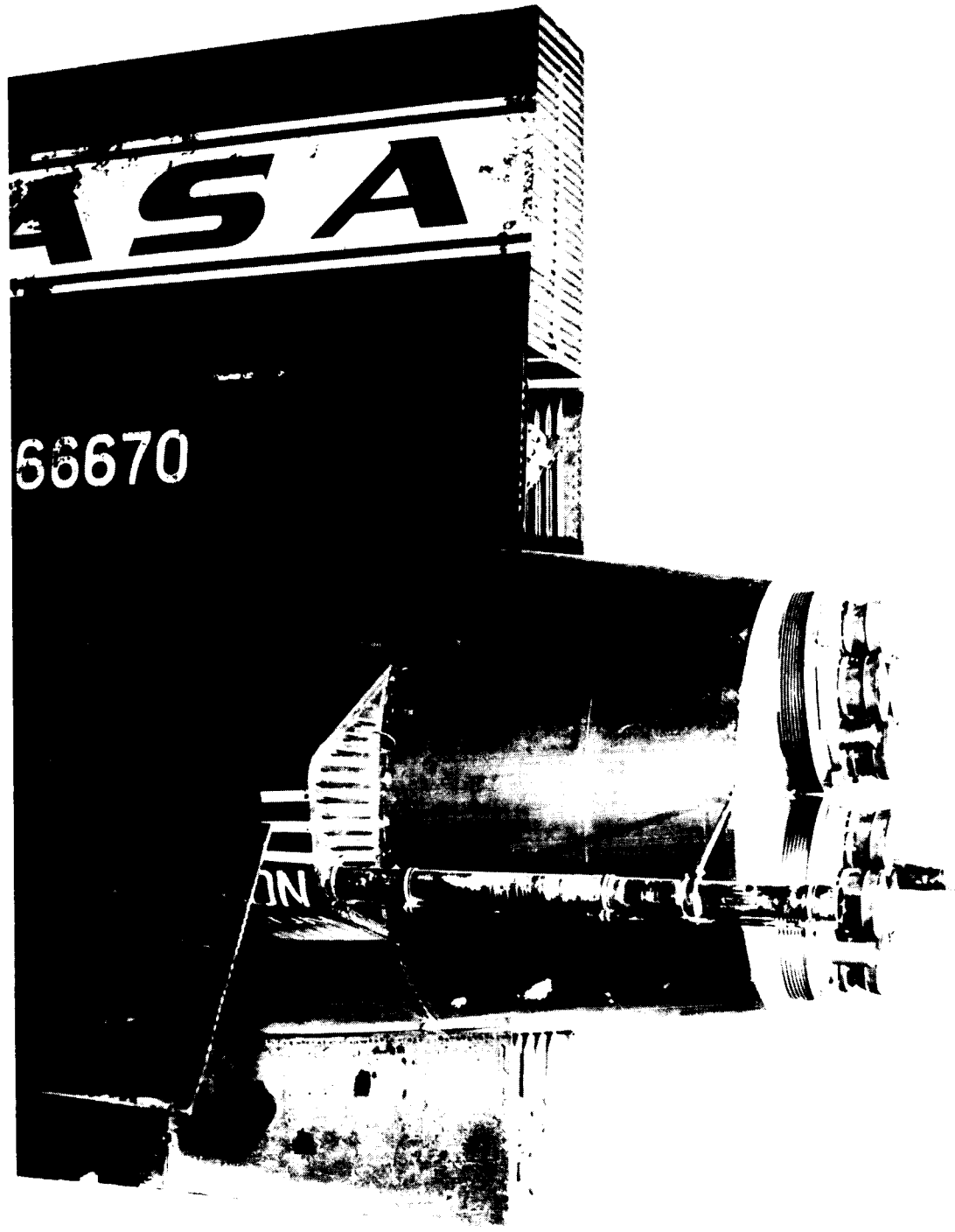

Figure 4.- X-15 viewed from the left rear. Lower jettisonable vertical fin has been removed. E-6646

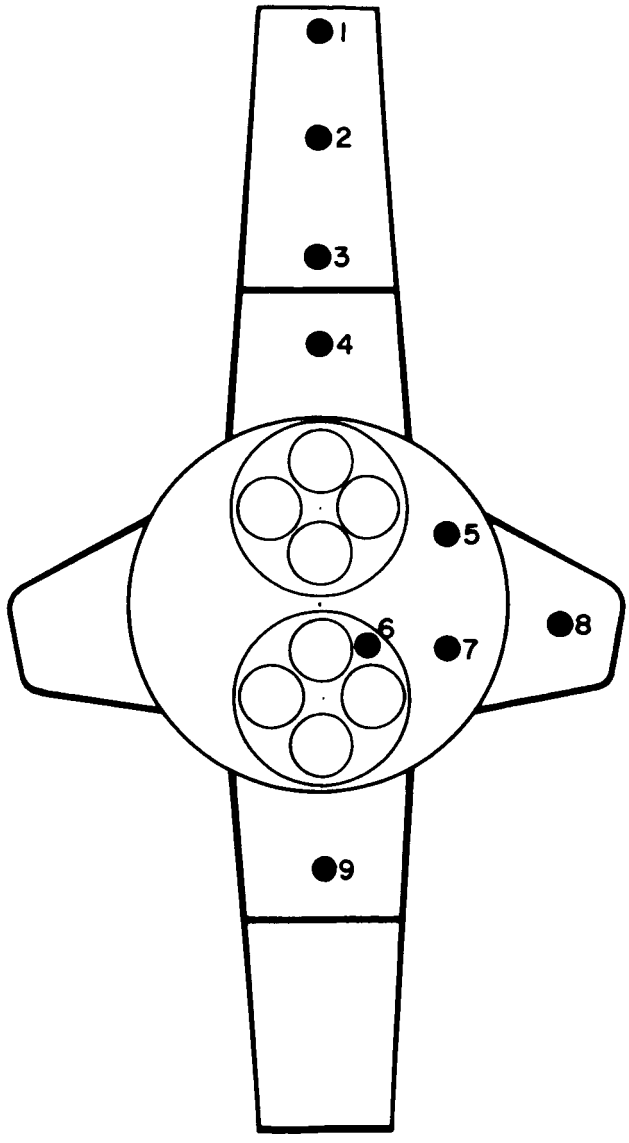

Orifice	1	2	3	4	5	6	7	8	9
Flight A		x		x	x	x	x	x	x
Flight B	x	x	x	x	x	x		x	
d, in.	35	35	35	35	10	3.5	10	44	35

Figure 5.- Schematic drawing of X-15 base showing location of orifices, with the interim-engine installation. (Not drawn to scale.)

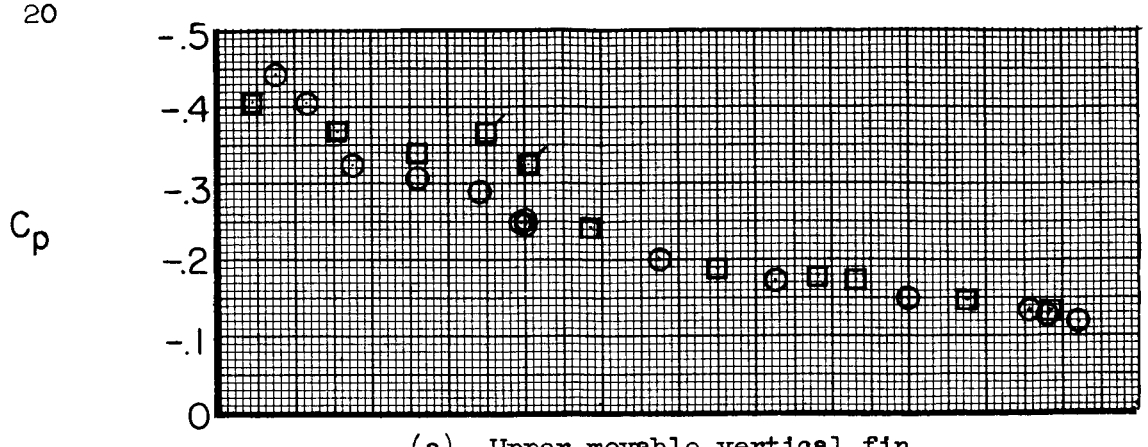

(a) Upper movable vertical fin.

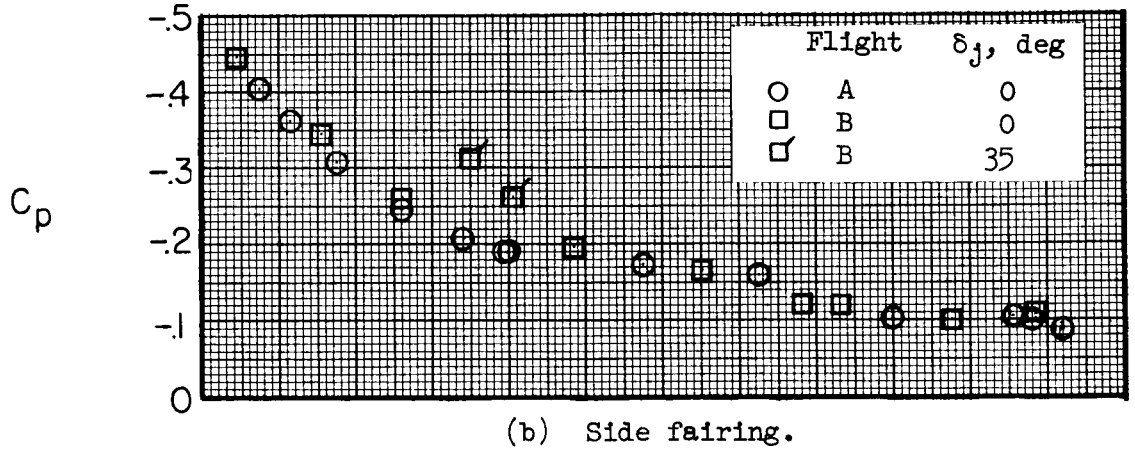

(b) Side fairing.

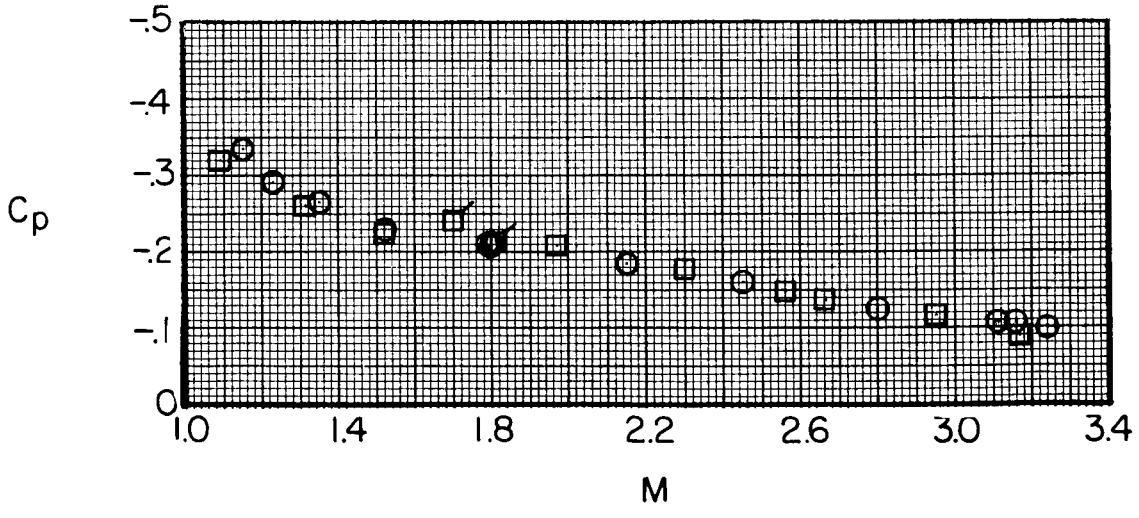

(c) Fuselage.

Figure 6.- Variation of base pressure coefficient with Mach number. Power off.

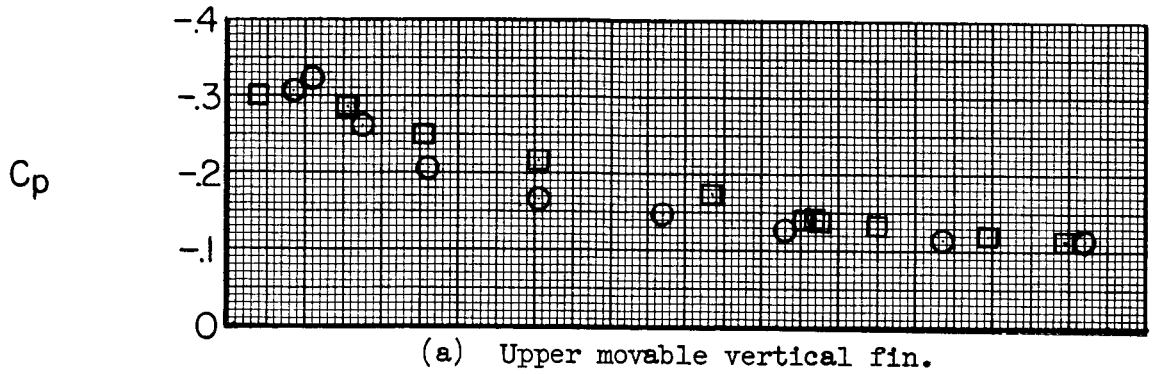

(a) Upper movable vertical fin.

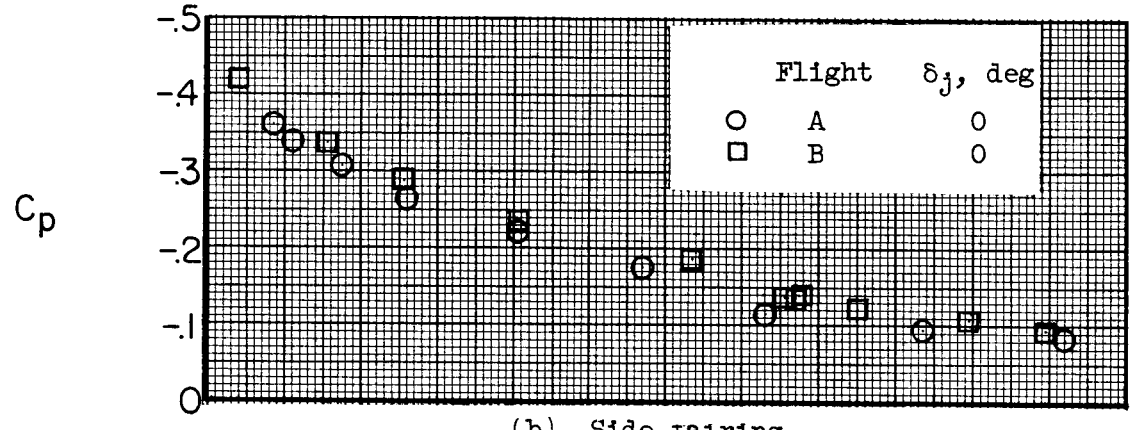

(b) Side fairing.

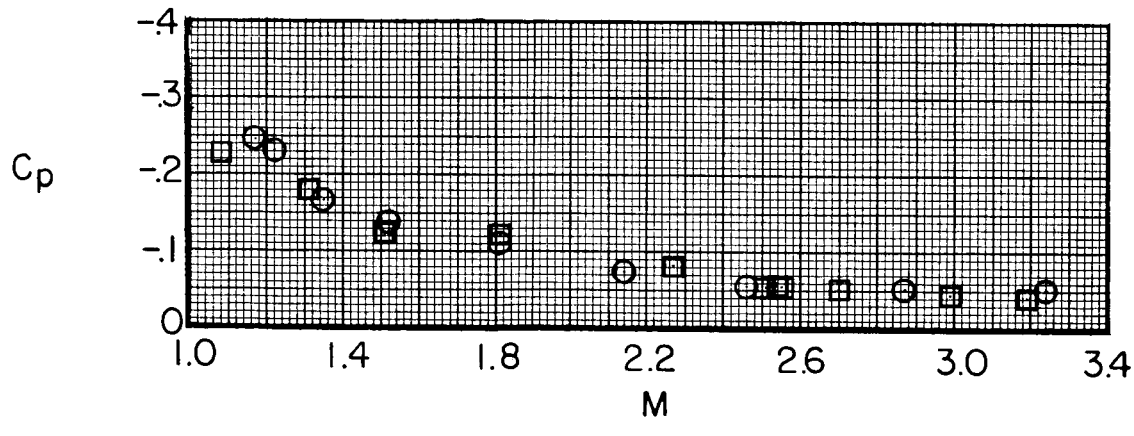

(c) Fuselage.

Figure 7.- Variation of base pressure coefficient with Mach number. Power on.

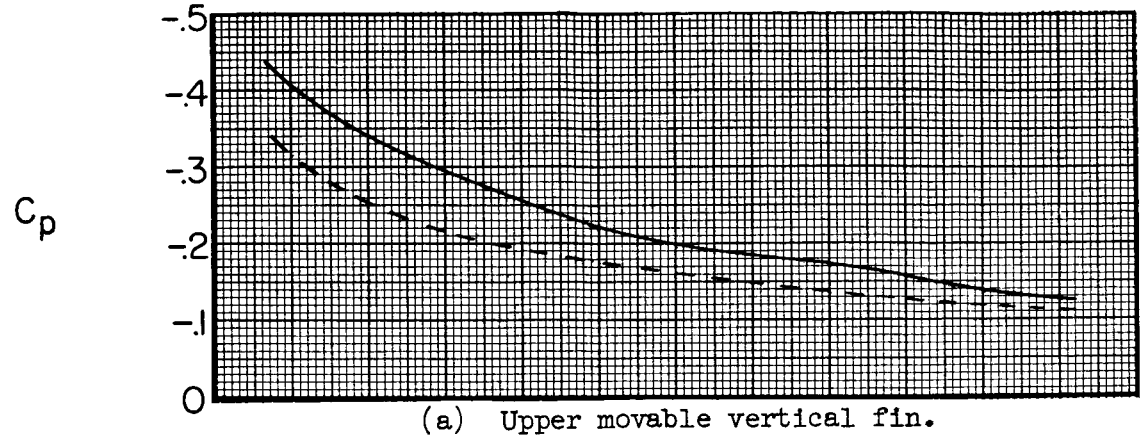

(a) Upper movable vertical fin.

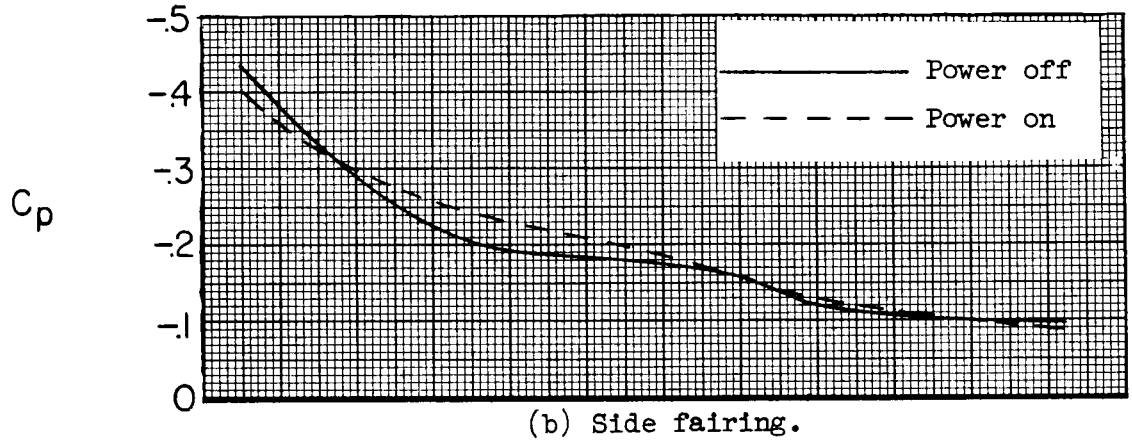

(b) Side fairing.

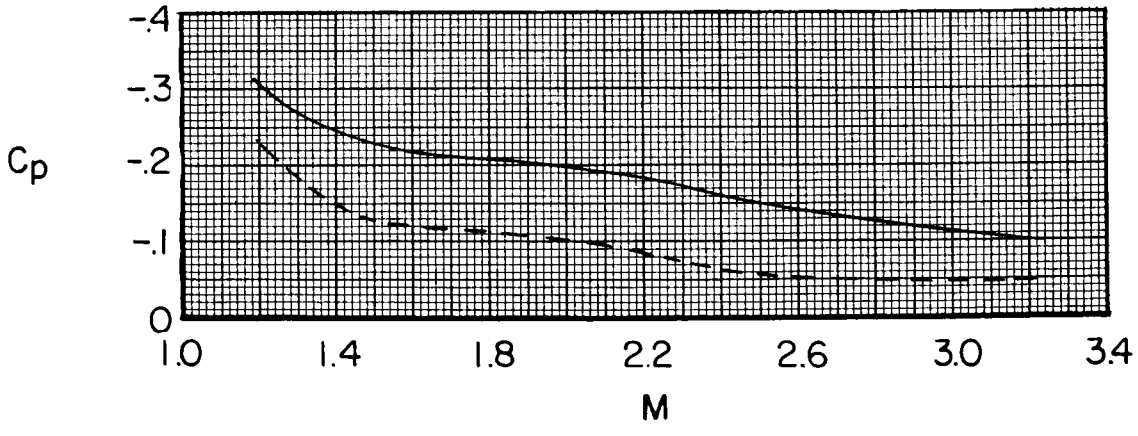

(c) Fuselage.

Figure 8.- Comparison of power-off and power-on base pressure coefficients.

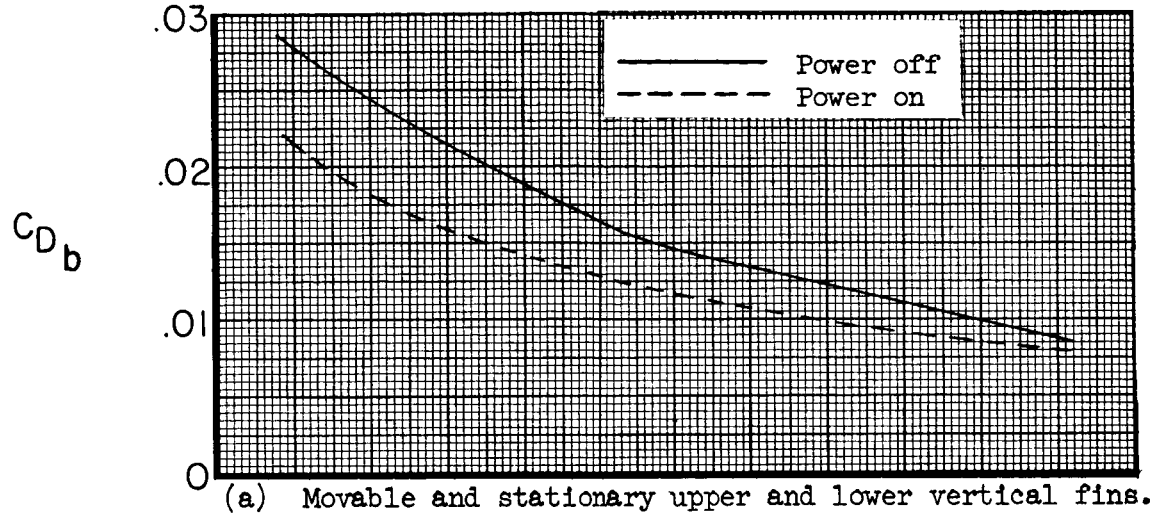

(a) Movable and stationary upper and lower vertical fins.

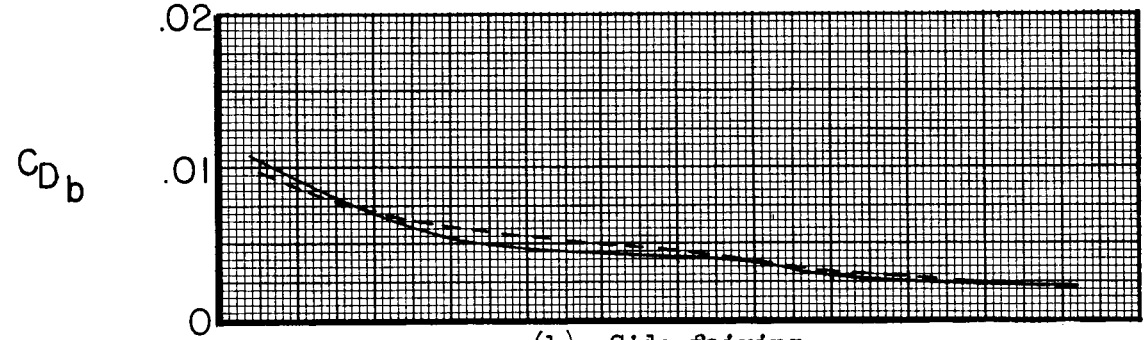

(b) Side fairing.

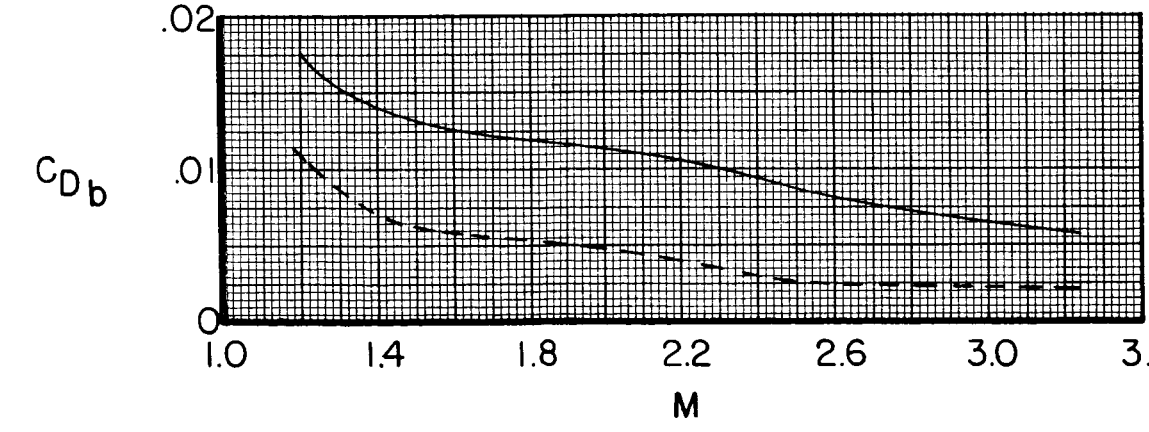

(c) Fuselage.

Figure 9.- Comparison of power-off and power-on base drag coefficients.

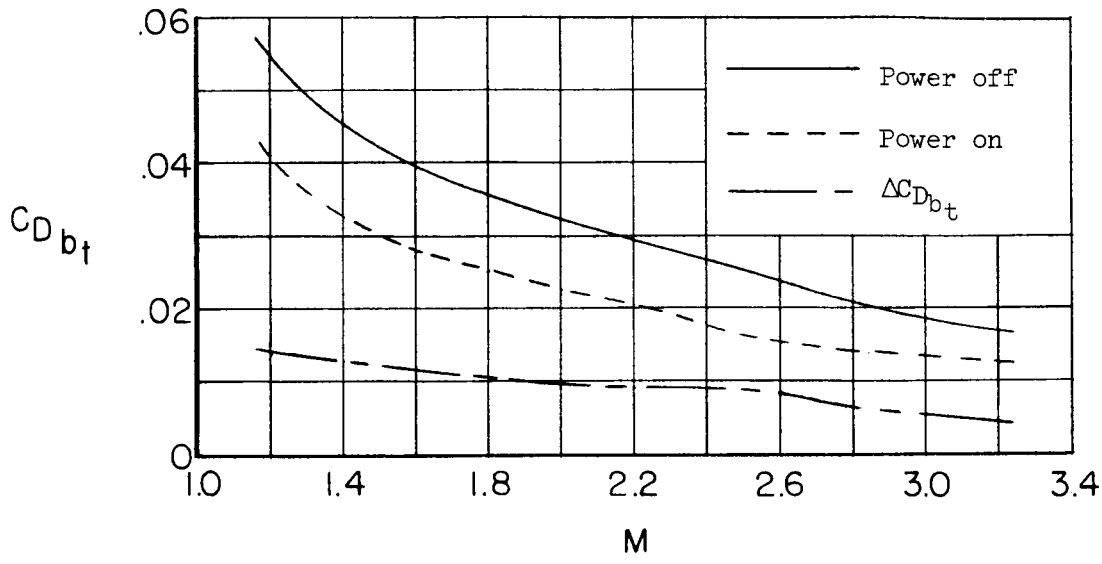

Figure 10.- Variation of total base drag coefficient of all base elements with Mach number.

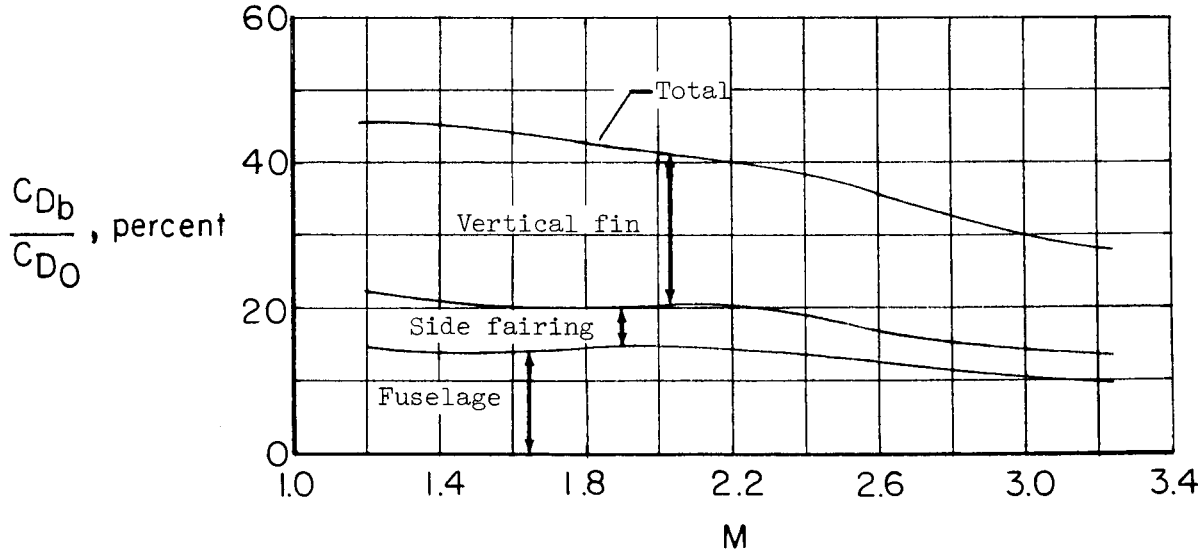

Figure 11.- Relationship of base drag coefficient to overall zero lift-drag coefficient. Power off

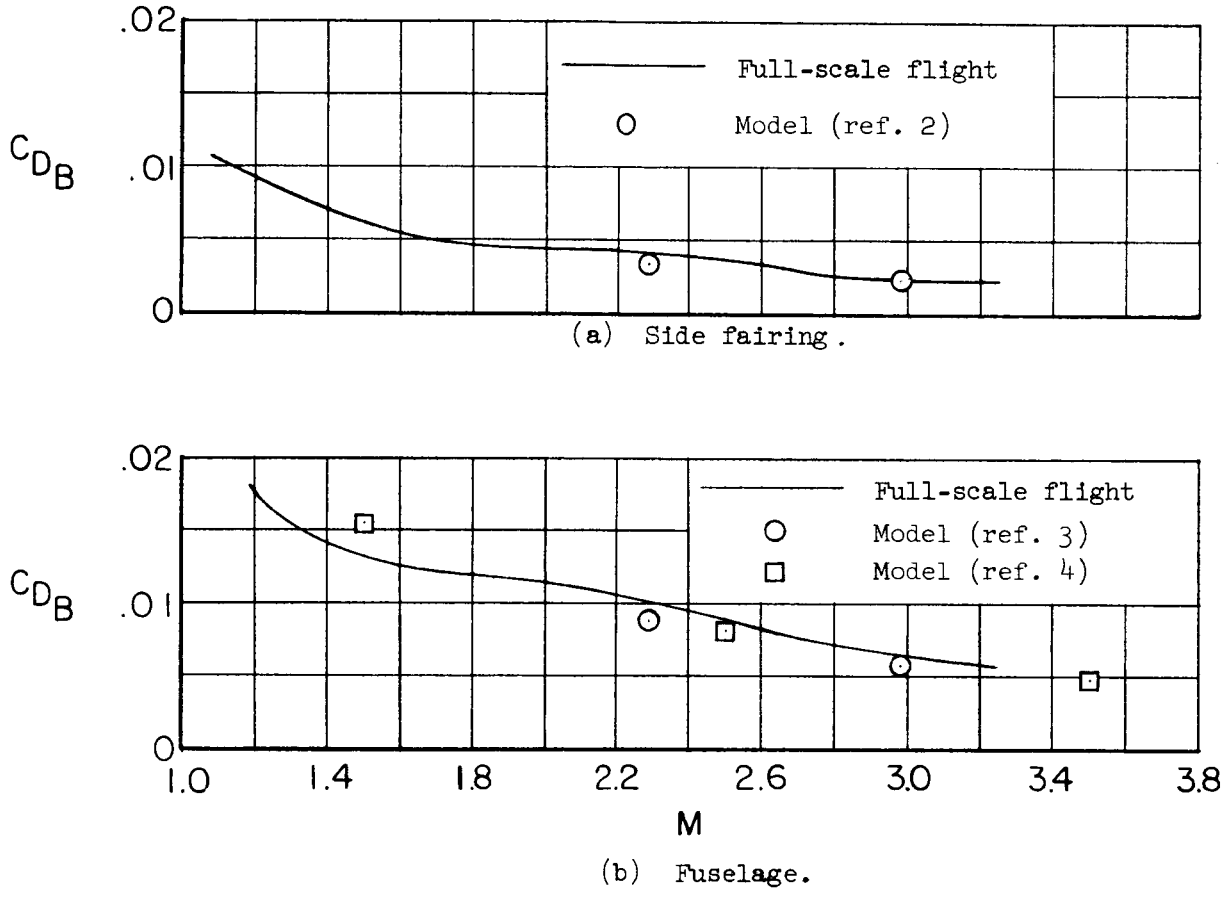

(a) Side fairing.

(b) Fuselage.

Figure 12.- Comparison of base drag coefficient with X-15 model results. Power off.

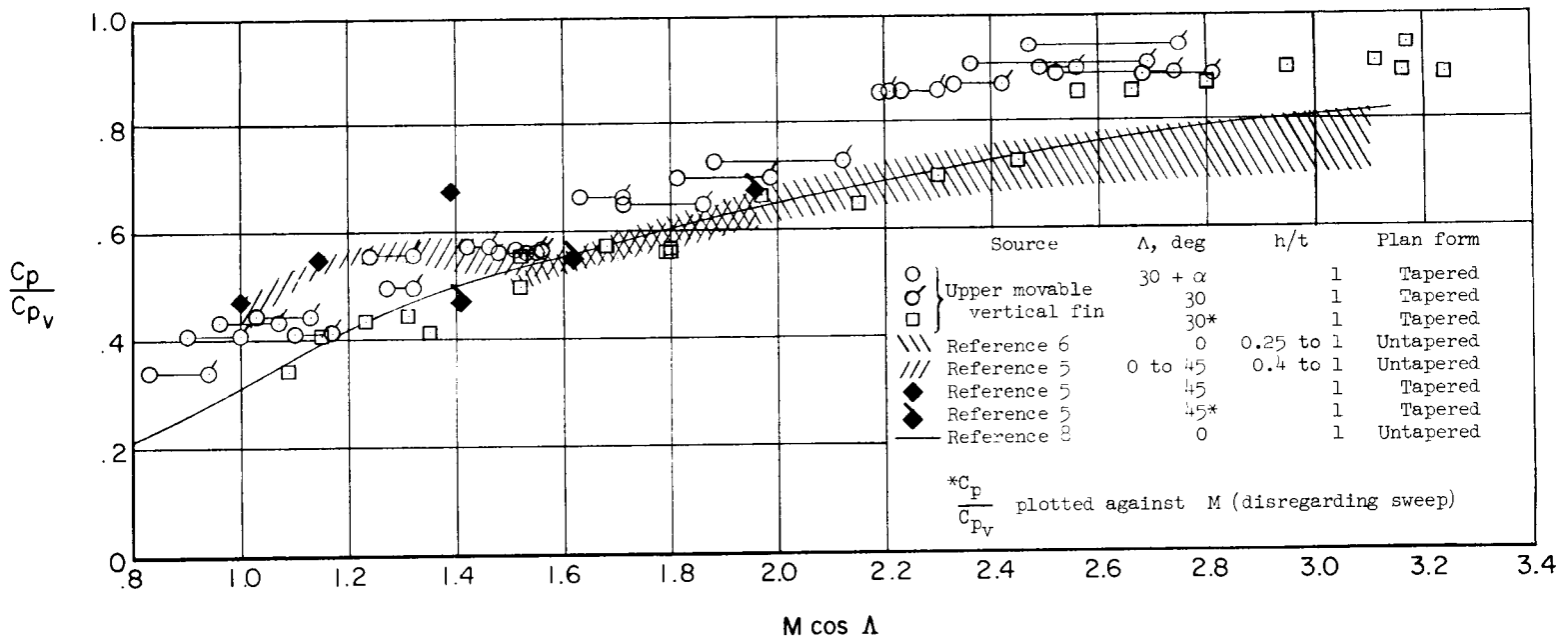

Figure 13.- Comparison of base pressure data for upper movable vertical fin with results from other investigations. Turbulent flow; power off for full-scale flight data.

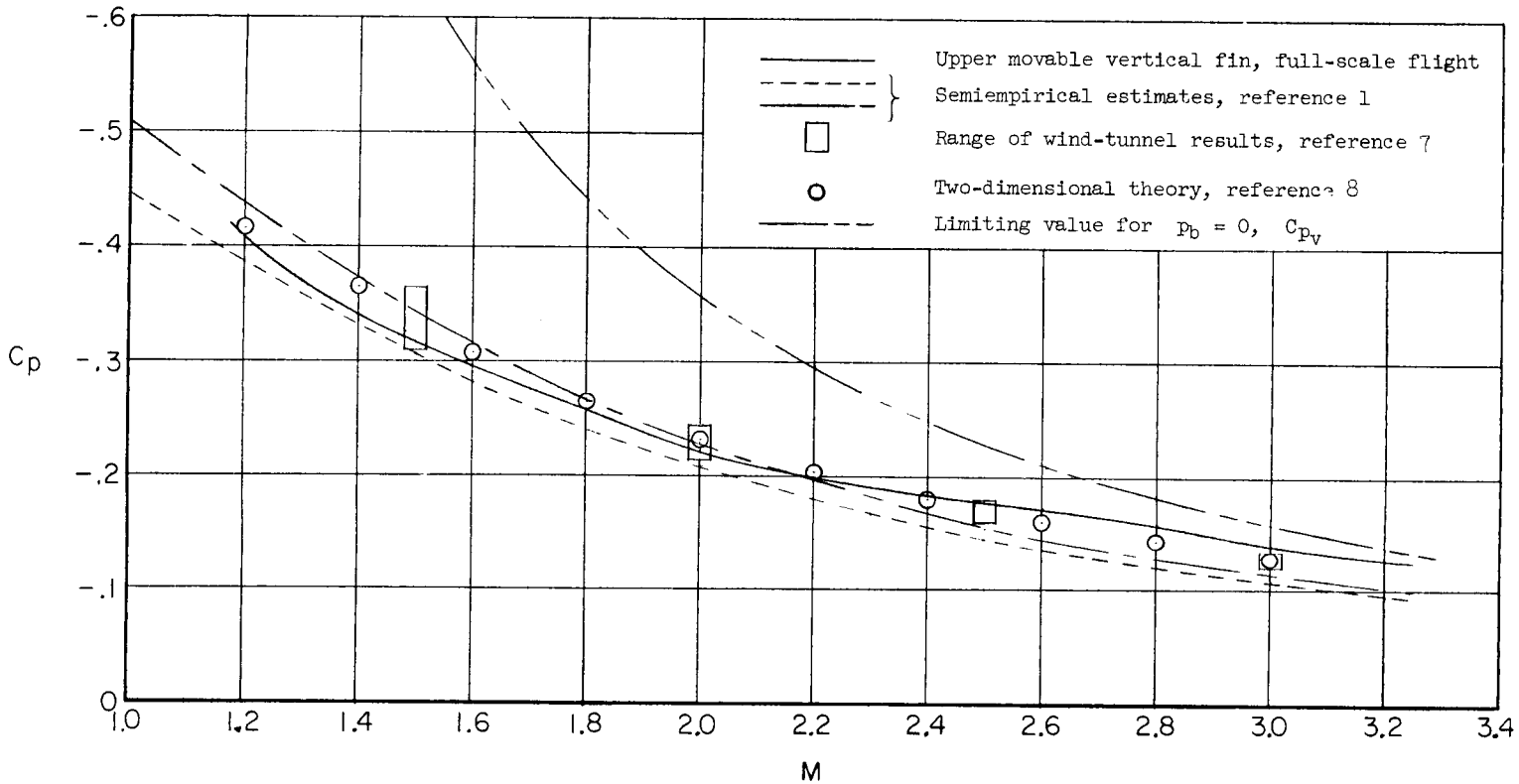

Figure 14.- Comparison of base pressure coefficient for upper movable vertical fin with wind-tunnel results, estimates, and theory. Turbulent flow; power off for full-scale flight data.

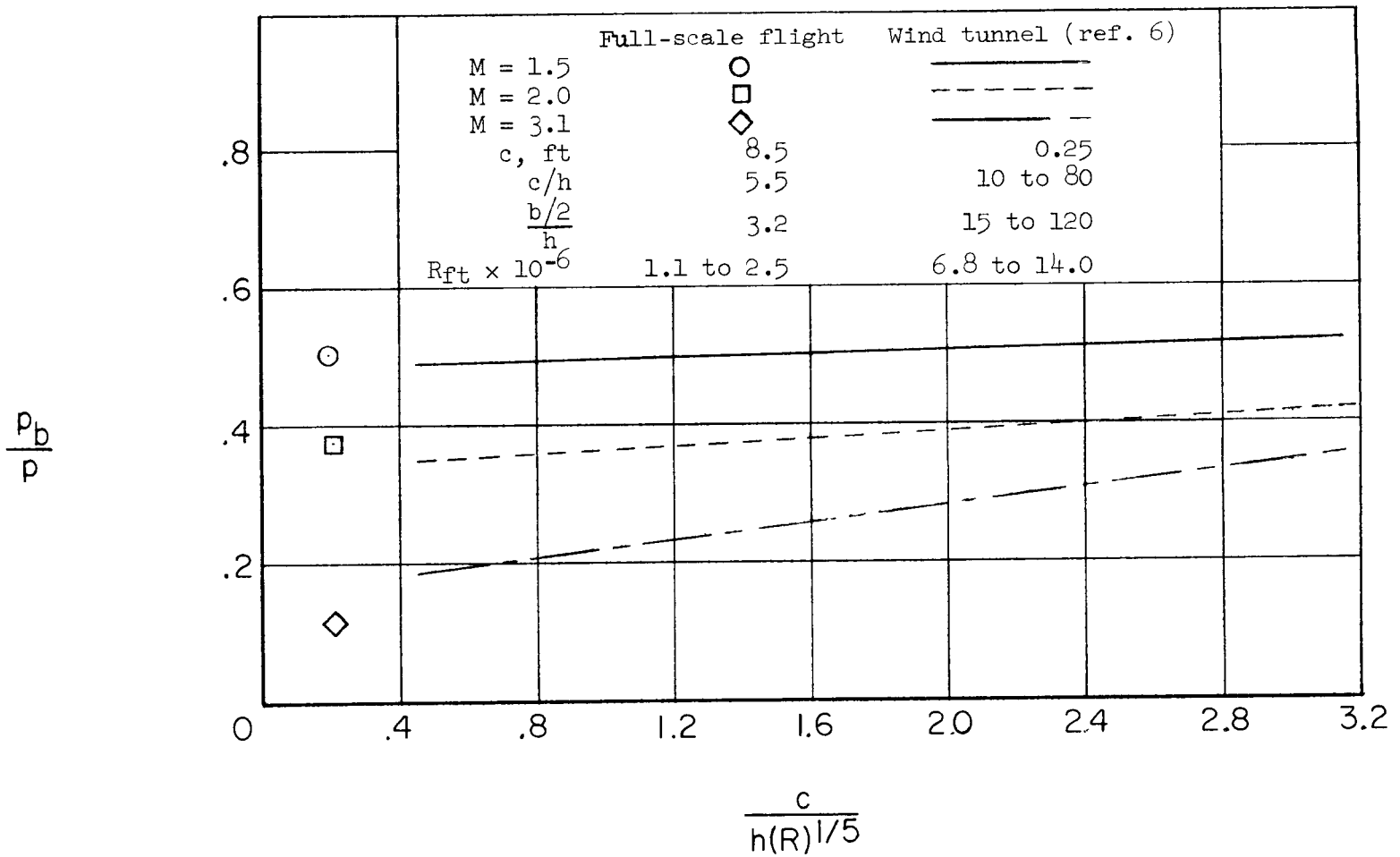

Figure 15.- Comparison of base pressure ratio for upper movable vertical fin and small-scale blunt-trailing-edge wings. Turbulent flow; power off for full-scale flight data.